1. Mariusz MAZUREK[3], 2. Marcin DZIADOSZ[4], 3. Grzegorz KŁOSOWSKI[4],
4. Dariusz WÓJCIK[1,2], 5. Krzysztof KRÓL[1,2]

Research & Development Center Netrix S.A. Lublin (1)
WSEI University, Lublin (2)
Polish Academy of Science, Warsaw (3)
Lublin University of Technology, Lublin (4)

ORCID: 1. 0000-0002-9646-6897 2. 0000-0002-0506-6653 3. 0000-0001-7927-3674 4. 0000-0002-4200-3432 5. 0000-0002-0114-2794

Application of electrical tomography in technological processes

Abstract. The article focuses on developing an advanced electrical impedance tomography (EIT) system designed for optimizing and controlling technological processes. The authors present an innovative tomographic system that integrates modern hardware solutions with sophisticated signal processing techniques and machine learning algorithms, specifically multi-branch neural networks.

Streszczenie. Artykuł koncentruje się na opracowaniu zaawansowanego systemu tomografii impedancji elektrycznej (EIT) przeznaczonego do optymalizacji i kontroli procesów technologicznych. Autorzy przedstawiają innowacyjny system tomograficzny, który integruje nowoczesne rozwiązania sprzętowe z zaawansowanymi technikami przetwarzania sygnałów oraz algorytmami uczenia maszynowego, w szczególności z wykorzystaniem wielogałęziowych sieci neuronowych (Zastosowanie tomografii elektrycznej w procesach technologicznych).

Keywords: Electrical impedance tomography (EIT), neural networks, image reconstruction, process control
Słowa kluczowe: Tomografia impedancji elektrycznej (EIT), sieci neuronowe, rekonstrukcja obrazów, kontrola procesów technologicznych

Introduction

This research presents an innovative tomographic system combining modern hardware technologies, sophisticated signal processing methods, and machine learning algorithms. The goal was to design a system capable of non-invasive, real-time monitoring of production environments, enabling enhanced diagnostics and control in a range of industrial settings [1-6]. Key to this approach was the integration of advanced microcontroller architectures and FPGA systems, which ensure the system can handle large volumes of data at high speeds, facilitating real-time analysis and remote reconfigurability. These features make the system highly adaptable, supporting a wide array of applications across different industries.

A major focus of the research was the development of image reconstruction algorithms based on multi-branch neural networks, which have proven effective in handling complex data and improving the quality and accuracy of tomographic reconstructions. The multi-branch configuration divides data processing across several independent branches, each focusing on different signal aspects, before combining the results to produce highly detailed and accurate images. To evaluate the relative effectiveness of the multi-branch configuration, an additional model was constructed and trained based on a single-layer LSTM neural network [7].

Fig.1. Tomograph with a test tank and settings: excitation frequency 10kHz, excitation current 1mA, number of sampling periods 3. Number of measurement electrodes 32. Configuration of measurement electrodes 2x16. 2.5D measurement sequence.

This allowed for a direct evaluation of the impact of the convolutional layers on the reconstruction process, thereby providing a more comprehensive understanding of each architectural configuration's relative strengths and limitations. By comparing the performance of the multi-branch neural networks with the LSTM model, the research sheds light on the benefits of using advanced network architectures for tomographic image reconstruction [8,9]. The research results demonstrate the potential of this integrated tomography system in industrial diagnostics and quality control. The application of multi-branch neural networks for image reconstruction, combined with the flexibility of modern hardware, opens up new opportunities for process engineering and production control. The developed system offers improved accuracy and efficiency in monitoring production processes, paving the way for more innovative and sustainable industrial operations [1].

Materials and methods

The tests were conducted using a hybrid tomography system specifically developed at the Netrix SA laboratory (Fig. 1). The system included a tomograph with a test tank that employed 32 measurement electrodes arranged in a 2x16 configuration to perform a 2.5D measurement sequence.

The key element is a measurement system based on microcontroller architecture using advanced FPGA systems. This system was designed for high flexibility and interoperability, enabling precise acquisition, sampling, and processing of signals in real time. FPGA microcontrollers allowed for dynamic reconfiguration of the system depending on the requirements specific to various research materials and technological processes. The project focused on developing an efficient communication interface that enables quick data exchange between the elements of the measurement system and the workstation. This interface ensures the transmission of measurement data and allows remote control of measurement parameters and system configuration. The use of the universal UART permitted protocol for easy integration of the tomography system with PC computers and mobile devices.

The central point of the methodology is the use of innovative image reconstruction algorithms based on machine learning. The work used multi-branch neural

networks to process tomographic data and generate high-resolution images of cross-sections of the examined objects. These algorithms were trained and verified on simulated measurement data, which allowed for the optimization of the image reconstruction process and increased accuracy and reliability of the results. A data set was constructed to emulate real measurements, thereby enabling the models to train and perform more effectively in authentic real-world scenarios.

#	Name	Type	Activations
1	sequence Sequence input with 448 dimensions	Sequence Input	896(C) × 1(B) × 1(T)
2	bilstm_1 BiLSTM with 1024 hidden units	BiLSTM	2048(C) × 1(B)
3	batchnorm_1 Batch normalization with 2048 channels	Batch Normalization	2048(C) × 1(B)
4	dropout_1 50% dropout	Dropout	2048(C) × 1(B)
5	fc_1 256 fully connected layer	Fully Connected	256(C) × 1(B)
6	tanh_1 Hyperbolic tangent	Tanh	256(C) × 1(B)
7	batchnorm_2 Batch normalization with 256 channels	Batch Normalization	256(C) × 1(B)
8	dropout_2 50% dropout	Dropout	256(C) × 1(B)
9	fc_2 256 fully connected layer	Fully Connected	256(C) × 1(B)
10	tanh_2 Hyperbolic tangent	Tanh	256(C) × 1(B)
11	batchnorm_3 Batch normalization with 256 channels	Batch Normalization	256(C) × 1(B)
12	dropout_3 50% dropout	Dropout	256(C) × 1(B)
13	fc_3 256 fully connected layer	Fully Connected	256(C) × 1(B)
14	tanh_3 Hyperbolic tangent	Tanh	256(C) × 1(B)
15	batchnorm_4 Batch normalization with 256 channels	Batch Normalization	256(C) × 1(B)
16	dropout_4 50% dropout	Dropout	256(C) × 1(B)
17	concat Concatenation of 3 inputs along dimensi...	Concatenation	768(C) × 1(B)
18	bilstm BiLSTM with 1280 hidden units	BiLSTM	2560(C) × 1(B)
19	batchnorm_5 Batch normalization with 2560 channels	Batch Normalization	2560(C) × 1(B)
20	fc_5 14100 fully connected layer	Fully Connected	14100(C) × 1(B)

Fig.2. Layers of the multi-branch neural networks

#	Name	Type	Activations
1	sequence Sequence input with 448 dimensions	Sequence Input	896(C) × 1(B) × 1(T)
2	lstm LSTM with 6144 hidden units	LSTM	6144(C) × 1(B) × 1(T)
3	batchnorm Batch normalization with 6144 channels	Batch Normalization	6144(C) × 1(B) × 1(T)
4	gmpool1d 1-D global max pooling	1-D Global Max Poo...	6144(C) × 1(B)
5	fc_2 14100 fully connected layer	Fully Connected	14100(C) × 1(B)

Fig.3. Layers of the LSTM networks

The input vector to the neural network was composed of 448 measurements, while the output was a three-dimensional image generated on a tetrahedral mesh comprising 14,100 finite elements. The training set comprised 30,000 observations, while the validation set included 3,000 observations, ensuring a robust training process. The structure of the multi-branch neural network, as illustrated in Figure 2, was purposely devised to address the tomographic data's intricacies and enhance the reconstructed images' overall quality. The second model, a single-branch LSTM network, comprised an input layer with 448 dimensions, followed by an LSTM layer with 6,144 hidden units, as illustrated in Fig. 3.

Fig. 4 clearly illustrates the branching points in the multi-branch architecture. Subsequent to the initial sequence and LSTM layer, the network divides into multiple branches. Each branch processes the data independently through additional layers, such as batch normalization and dropout. After the independent processing of the branches is complete, the branches are merged using a technique known as concatenation.

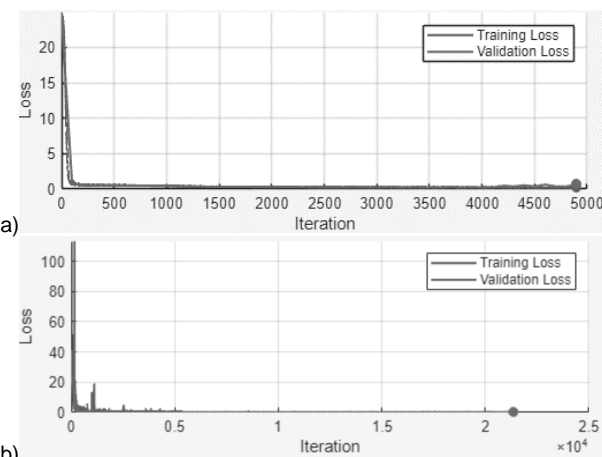Fig.4. Branching structure in a multi-branch neural network

Fig.5. The training performance of neural networks: a) multi-branch, b) LSTM

Concatenation is a technique whereby the outputs from different branches are combined by joining them into one longer vector. To illustrate, if branch A generates a vector of length c and branch B generates a vector of length d, the result of the concatenation is a vector of length c+d. This method guarantees that all information from both branches is preserved without any mathematical mixing, thus maintaining the distinct contributions of each branch.

The concatenated vector is then processed by the subsequent layer, which is a bidirectional LSTM layer. This layer contains 1280 hidden units, which facilitate sophisticated sequential processing. The substantial number of hidden units permits the network to more effectively capture the hidden dependencies between inputs and outputs, thereby enhancing the model's capacity to accurately identify patterns and relationships in the tomographic data, leading to more precise reconstructions.

To ensure a good comparison, the training process for both the multi-branch neural network and the single-branch LSTM network was conducted using identical parameters. The training process for each network was conducted for a maximum of 500 epochs with a mini-batch size of 128. This approach facilitated the efficient processing of data and timely updating of weights in the models. The Adam optimization algorithm was employed to minimize the loss function. The validation data were evaluated at each 100th iteration to monitor the model's performance and prevent overfitting. A patience threshold of eight validation checks was established, indicating that training would conclude prematurely in the event that the model demonstrated an

inability to enhance its performance after eight consecutive validations.

As illustrated in Fig. 5, the graphs demonstrate the training performance of the models. In both plots, the smooth decline in loss values and the absence of significant fluctuations indicate that the training process is proceeding in an optimal manner. This suggests that the model is approaching a state of convergence and that there is no evidence of overfitting. The consistency between the training and validation loss curves provides further proof of the robustness of the model, thereby reinforcing confidence in its capacity to generalize to new data.

Results

The presented research results demonstrate the effectiveness of the developed tomographic system in monitoring and analyzing production processes. The use of advanced image reconstruction algorithms allowed for the detection of subtle changes in the material and improved the quality and accuracy of tomographic images.

Table 1 presents a comparison of the reconstruction results generated by two different models: the multi-branch neural network model and the LSTM model. Each row corresponds to a different test case, designated by the numbers 1 to 4. The comparison is based on the degree of similarity between the reconstructed image and the reference pattern. Each figure in Table 1 is presented from a 3D isometric view and a top view. This dual representation offers a more comprehensive visualization of the reconstructed images, enabling a clearer comparison between the reference pattern and the reconstructions produced by the multi-branch neural network and LSTM models.

Since visualizations alone are insufficient for a thorough assessment, quantitative metrics were employed to enhance the objectivity of the evaluations. These metrics include Mean Squared Error (MSE), Peak Signal-to-Noise Ratio (PSNR), Structural Similarity Index (SSIM), and Image Correlation Coefficient (ICC) [10].

Each of these indicators provides distinct insights into the quality of the reconstructions. The MSE is calculated as:

$$MSE = \sum_{i=1}^{R} \frac{(\hat{y}_i - y_i)^2}{R}$$

(1)

Where: y_i - the pattern voxel value (the intensity of the i-th voxel), $\hat{y}_i$ - the corresponding reconstructed voxel value (the intensity of the i-th voxel), R - the total number of voxels in the 3D image. MSE measures the average squared difference between the reference and reconstructed values, with lower values indicating better accuracy of the reconstruction.

The PSNR is used to assess the ratio of the maximum possible signal power to the power of corrupting noise, computed as:
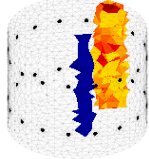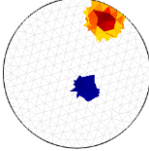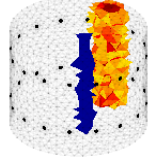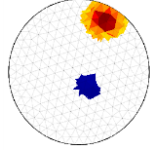
(2) $$PSNR = 10 \cdot log_{10}(R^2/MSE)$$
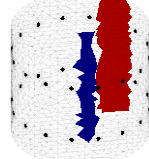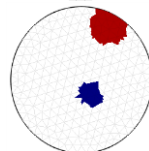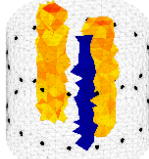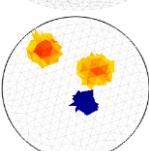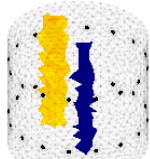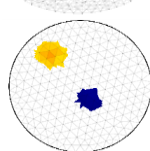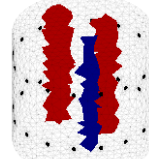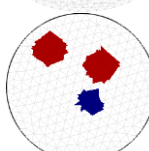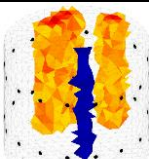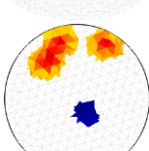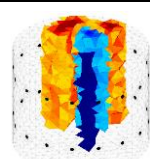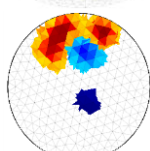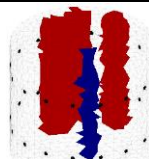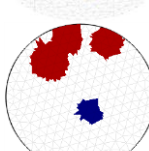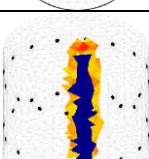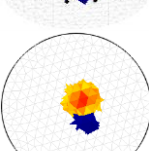
The SSIM (Structural Similarity Index) is formulated to assess image quality based on the human visual perception of structural information. It compares the reference and reconstructed images' luminance, contrast, and structure. SSIM values closer to 1 reflect better structural similarity.

$$SSIM = \frac{(2\mu_{\hat{y}}\mu_y + C_1)(2\sigma_{\hat{y}y} + C_2)}{(\mu_{\hat{y}}^2 + \mu_y^2 + C_1)(\sigma_{\hat{y}}^2 + \sigma_y^2 + C_2)}$$
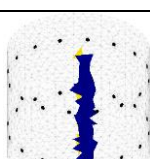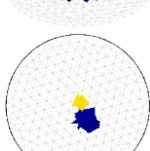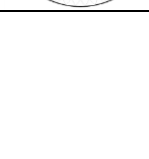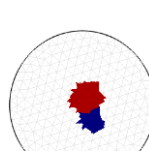
(3)

where: $\mu_{\hat{y}}, \mu_y$ - the local means, $\sigma_{\hat{y}}, \sigma_y$ - the standard deviations, $\sigma_{\hat{y}y}$ - the cross-covariance for the images, C_1

$= (0.01*L)^2$, $C_2 = (0.03*L)2$, L is set to 1 for normalized voxel values in the range (0,1).

Table 1. Comparison of the reconstructions generated by multi-branch neural networks and LSTM model

Finally, the ICC (Image Correlation Coefficient) quantifies the correlation between the reference and reconstructed images. It is calculated as:

$$ICC = \frac{\sum_{i=1}^{R}(y_i - \bar{y})(\hat{y}_i - \bar{\hat{y}})}{\sqrt{\sum_{i=1}^{R}(y_i - \bar{y})^2 \sum_{i=1}^{R}(\hat{y}_i - \bar{\hat{y}})^2}}$$

(4)

where: $\bar{y}$ - the average intensity values of the pattern, $\bar{\hat{y}}$ - the average intensity values of the reconstructed images

The results of these metrics are presented in Table 2, which compares the performance of the multi-branch neural networks and LSTM models across four test cases. The results demonstrate that the multi-branch neural networks

consistently achieve lower MSE values, indicating more accurate reconstructions. To illustrate, in test case #4, the MSE for the multi-branch neural networks is 0.089, which is markedly lower than the 0.155 for the LSTM model. This indicates that the multi-branch approach yields reconstructions of greater precision.

Table 2. Comparison of reconstruction quality metrics

Indicator	model	ID			
		#1	#2	#3	#4
MSE	multi-branch neural networks	**0.192**	**0.224**	**0.446**	**0.089**
	LSTM	0.202	0.324	0.688	0.155
PSNR	multi-branch neural networks	**7.171**	**6.492**	**3.508**	**10.466**
	LSTM	6.951	4.894	1.625	8.092
SSIM	multi-branch neural networks	**0.402**	**0.274**	0.419	**0.264**
	LSTM	0.400	0.268	**0.437**	0.249
ICC	multi-branch neural networks	**0.899**	**0.821**	**0.819**	**0.879**
	LSTM	0.885	0.730	0.787	0.792

The PSNR values confirm this observation, with higher values evident for the multi-branch neural networks across most test cases, particularly in test case #4, where the PSNR reaches 10.466, in contrast to 8.092 for the LSTM model. This suggests that the multi-branch model is more effective in reducing noise in the reconstructions. With regard to SSIM, the two models exhibit comparable performance, although the multi-branch neural networks demonstrate slight superiority in terms of structural similarity, particularly in test case #3, with an SSIM value of 0.419 compared to 0.437 for the LSTM model. Finally, the ICC values demonstrate that the multi-branch neural networks achieve higher correlations with the reference images across all test cases. In test case #4, for instance, the multi-branch neural networks achieve an ICC of 0.879, whereas the LSTM model records an ICC of 0.792. This highlights the enhanced precision of the multi-branch approach in reconstructing images that closely resemble the reference patterns.

The quantitative analysis presented in Table 2 clearly demonstrates that the multi-branch neural networks outperform the LSTM model in terms of reconstruction accuracy, noise reduction, structural similarity, and correlation with the reference image, particularly in more complex cases.

Conclusions

The conducted research provides a comprehensive examination of advanced EIT techniques with the objective of optimizing and controlling technological processes. The primary innovation is the integration of state-of-the-art hardware with advanced signal processing methods and machine learning algorithms, particularly the use of multi-branch neural networks for image reconstruction. The comparative analysis between the multi-branch neural networks and the LSTM model demonstrates that the multi-branch approach is more effective than the LSTM model in tomographic image reconstruction. The multi-branch neural networks demonstrate consistent superiority across all analyzed quality indicators, confirming their effectiveness in

delivering more accurate and reliable reconstructions. These findings confirm the potential of the proposed multi-branch model to enhance image quality and accuracy, rendering it highly suitable for real-world applications in diagnostics, process monitoring, and quality control.

Authors: *Mariusz Mazurek Ph.D., Institute of Philosophy and Sociology of the Polish Academy of Science Warsaw, Poland, E-mail: mmazurek@ifispan.edu.pl, Marcin Dziadosz M.Sc. Eng., Lublin University of Technology, Nadbystrzycka 38, Lublin, Poland, E-mail: m.dziadosz@pollub.pl; Grzegorz Kłosowski Ph.D., Lublin University of Technology, Nadbystrzycka 38A, Lublin, Poland, E-mail: g.klosowski@pollub.pl;, Dariusz Wójcik Ph.D. Eng., Faculty of Transport and Computer Science, WSEI University, Projektowa 4, 20-209 Lublin, Poland, Research&Development Centre Netrix S.A. Związkowa 26, 20-148 Lublin dariusz.wojcik@netrix.com.pl, Krzysztof Król M.Sc., Faculty of Transport and Computer Science, WSEI University, Projektowa 4, 20-209 Lublin, Poland, Research&Development Centre Netrix S.A. Związkowa 26, 20-148 Lublin, Email: krzysztof.krol@netrix.com.pl;*

REFERENCES

[1] Król K., Rymarczyk, T., Niderla K., Kozłowski E.: Sensor Platform of Industrial Tomography for Diagnostics and Control of Technological Processes. *Informatyka, Automatyka, Pomiary w Gospodarce i Ochronie Środowiska*, 13 (2023), No. 1, 33-37

[2] Przysucha B., Wójcik D., Rymarczyk T., Król K., Kozłowski E., Gąsior M.: Analysis of Reconstruction Energy Efficiency in EIT and ECT 3D Tomography Based on Elastic Net, *Energies*, 16 (2023), No.3, 1490

[3] Rybak G., Kozłowski E., Król K., Rymarczyk T., Sulimierska A., Dmowski A., Bednarczuk P.: Algorithms for Optimizing Energy Consumption for Fermentation Processes in Biogas Production, *Energies*, 16 (2023), No. 24, 7972

[4] Rymarczyk T., Kozłowski E., Kłosowski G.: Electrical Impedance Tomography in 3D Flood Embankments Testing – Elastic Net Approach. *Transactions of the Institute of Measurement and Control*, 42 (2020), No.4, 680-690

[5] Maciura, Łukasz, Wójcik, D., Rymarczyk, T., Król, K., Novel hybrid algorithm using convolutional autoencoder with SVM for electrical impedance tomography and ultrasound computed tomography. *Informatyka, Automatyka, Pomiary W Gospodarce I Ochronie Środowiska*, 13 (2023), No. 2, 4–9

[6] Panskyi T, Korzeniewska E, Firych-Nowacka A. Educational Data Clustering in Secondary School Sensor-Based Engineering Courses Using Active Learning Approaches. *Applied Sciences*, 14 (2024), No.12, 5071

[7] Kłosowski G, Rymarczyk T, Niderla K, Kulisz M, Skowron Ł, Soleimani M. Using an LSTM network to monitor industrial reactors using electrical capacitance and impedance tomography – a hybrid approach, *Eksploatacja i Niezawodnosc – Maintenance and Reliability*, 25 (2023). No.1, https://doi.org/10.17531/EIN.2023.1.11

[8] Kłosowski G., Rymarczyk T.: Application of Convolutional Neural Networks in Wall Moisture Identification by Eit Method. *Informatyka, Automatyka, Pomiary w Gospodarce i Ochronie Środowiska*, 12 (2022), 20-23.

[9] Wójcik D., Rymarczyk T., Przysucha B., Gołąbek M., Majerek D., Warowny, T., Soleimani, M.: Energy Reduction with Super-Resolution Convolutional Neural Network for Ultrasound Tomography, *Energies*, 16 (2023), 1387.

[10] Kulisz M., Kłosowski G., Rymarczyk T., Hoła A., Niderla K., Sikora J., The use of the multi-sequential LSTM in electrical tomography for masonry wall moisture detection, *Measurement*, 234 (2024) 114860.